materials

MDPI

Article

Thermoelectric Properties of Co-Substituted Al–Pd–Re Icosahedral Quasicrystals

Yoshiki Takagiwa

National Institute for Materials Science (NIMS), 1-2-1 Sengen, Tsukuba 305-0047, Japan; takagiwa.yoshiki@nims.go.jp

Abstract: The practical application of quasicrystals (QCs) as thermoelectric materials makes icosahedral (*i*-) Al–Pd–Re QC attractive because of its moderate electrical conductivity (~280 Ω^{-1} cm^{-1}), relatively high Seebeck coefficient (~100 μV K^{-1}), and low thermal conductivity (~1.3 W m^{-1} K^{-1}) at room temperature. To develop a thermoelectric Π-shaped power generation module, we need both p- and n-type thermoelectric materials. In this work, we aimed to develop an n-type *i*-Al–Pd–Re-based QC and investigated the effect of Co substitution for Re on the thermoelectric properties, i.e., the electron-doping effect. We synthesized dense bulk samples with nominal compositions of $Al_{71}Pd_{20}(Re_{1-x}Co_x)_9$ (x = 0, 0.1, 0.2, 0.3, 0.4, 0.5) via arc-melting, annealing, and sintering methods. We found that Co can produce n-type carriers in dilute substitution amounts of x = 0.1 and 0.2; however, the Seebeck coefficient at 300 K showed an n- to p-type transition with increasing x. This indicates that a simple rigid-band approximation is not applicable for *i*-Al–Pd–Re QC, which makes it difficult to synthesize an n-type *i*-Al–Pd–Re-based QC. Although the thermal conductivity was reduced from 1.28 (x = 0) to 1.08 W m^{-1} K^{-1} (x = 0.3) at 373 K by lowering of the electron thermal conductivity (electrical conductivity) and the alloying effect via Co substitution, the dimensionless figure of merit was not enhanced because of lowering of the power factor for all samples. The elastic moduli of *i*-Al–Pd–Re QC decreased by Co substitution, indicating that *i*-Al–Pd–Re-Co QC had a more ionic and brittle character.

Keywords: quasicrystals; thermoelectric materials; Al–Pd–Re–Co; electron doping

check for updates

Citation: Takagiwa, Y. Thermoelectric Properties of Co-Substituted Al–Pd–Re Icosahedral Quasicrystals. *Materials* **2022**, *15*, 6816. https://doi.org/10.3390/ma15196816

Academic Editor: Yuan Yu

Received: 9 September 2022
Accepted: 28 September 2022
Published: 30 September 2022

Publisher's Note: MDPI stays neutral with regard to jurisdictional claims in published maps and institutional affiliations.

Copyright: © 2022 by the author. Licensee MDPI, Basel, Switzerland. This article is an open access article distributed under the terms and conditions of the Creative Commons Attribution (CC BY) license (https://creativecommons.org/licenses/by/4.0/).

1. Introduction

From the viewpoint of highly efficient energy use, the importance of thermoelectric conversion technology that directly converts thermal energy into electrical energy is increasing. There are many reports on research and development related to various high-performance thermoelectric materials [1] and modularization technology [2]. The dimensionless figure of merit (zT) is an evaluation index for a thermoelectric material, expressed as:

$$zT = \frac{S^2\sigma}{\kappa_{\text{total}}}T, \quad (1)$$

where S, σ, κ_{total}, and T are the Seebeck coefficient, electrical conductivity, total thermal conductivity, and temperature, respectively [3,4]. Here, κ_{total} is the sum of two contributions: the electron contribution, κ_{electron}, and the phonon contribution, κ_{phonon}, i.e.,

$$\kappa_{\text{total}} = \kappa_{\text{electron}} + \kappa_{\text{phonon}} \quad (2)$$

κ_{electron} is proportional to σ through the Wiedemann–Franz law:

$$\kappa_{\text{electron}} = L_0\sigma T, \quad (3)$$

where L_0 is the Lorenz number. Thus, both optimizing S and σ and lowering κ_{phonon} are necessary to enhance the zT value. Relevant materials designs, such as band engineering

and valleytronics [5], can improve the power factor ($S^2\sigma$), and nano-structuring [6] and phonon engineering [2] can be employed to reduce κ_{phonon}.

In recent years, the application of thermoelectric materials as autonomous power supplies to drive Internet-of-Things (IoT) devices [7] has become possible [8,9]. The usable temperature range is below 200 °C, as derived from environmental heat sources and low-temperature waste heat, and it is crucial to ensure a temperature difference when using thermoelectric power generation modules. For this purpose, the κ_{total} of a material-forming thermoelectric module should be low, i.e., less than a few W m^{-1} K^{-1} at operating temperature. In contrast, a high output voltage is required when driving IoT devices with a DC–DC converter; thus, a high S is required for the material.

Icosahedral quasicrystals (*i*-QCs) exhibit interesting electrical and thermal transport properties [10], and their applications [11] vary in structural materials [12], thermal rectifiers [13], and thermoelectric materials [14]. Regarding thermoelectric applications, *i*-Al–Pd–Re QC has been widely investigated from experimental [14] and theoretical [15] points of view. The *i*-Al–Pd–Re QC exhibits promising thermoelectric properties because of its moderate σ (~280 Ω^{-1} cm^{-1}), relatively high S (~100 μV K^{-1}), and low κ_{total} (~1.3 W m^{-1} K^{-1}) at room temperature [16], which are brought about by pseudo-gap formation at the Fermi energy (E_F) [17] and their complex crystal structures with icosahedral symmetry [18]. Recently, we obtained a relatively large zT_{max} value of 0.26 at 573 K for the Fe-substituted Al–Pd–Re system [16]: 2/1-Al–Pd–Re–Fe approximant crystal showed the highest $S^2\sigma$ of ~900 μW m^{-1} K^{-2} at 573 K. To date, we have succeeded in improving the thermoelectric performance of only p-type materials based on *i*-Al–Pd–Re QC [14,16] and isostructural *i*-Al–Pd–Mn QC [19,20].

To develop a robust thermoelectric Π-shaped power generation module, we need both p- and n-type thermoelectric materials with good mechanical properties. In this work, we aimed to develop an n-type *i*-Al–Pd–Re-based QC. We selected Co as an electron dopant because Co has a larger number of valence electrons than Re. Regarding the Al–Pd–Co ternary system, there is one report on the thermoelectric properties of 1/1-cubic approximant crystal [21]. This paper reports the effect of Co substitution for Re in *i*-Al–Pd–Re QC on the thermoelectric and mechanical properties.

2. Methods and Materials

Mother ingots of nominal compositions of $Al_{71}Pd_{20}(Re_{1-x}Co_x)_9$ (x = 0, 0.1, 0.2, 0.3, 0.4, 0.5) were synthesized by an arc-melting technique under a purified argon atmosphere (NEV-AD03TC; Nisshin Giken Co., Japan) using the starting materials Al (powder, 99.99%), Pd (powder, 99.9%), Re (powder, 99.9%), and Co (powder, >99%). The obtained bulk samples were annealed at 1223 K for 24 h under a purified argon atmosphere to prevent oxidization (MILA-5000; Advance Riko, Inc., Yokohama, Japan). The annealed samples were hand-milled in ethanol using an agate mortar and pestle. The hand-milled powder samples were sieved using a stainless-steel sieve of 45 μm mesh and then placed in a carbon die with an inner diameter of 10 mm for spark plasma sintering (SPS) (LABOX-110MC; SinterLand, Inc., Nagaoka, Japan) under a purified argon atmosphere. The applied pressure was set to 115 MPa during the sintering process to synthesize dense bulk samples. This value is twice as high as a condition that previously achieved a high relative density above 90% for *i*-Al–Pd–Re QC [22]. To obtain dense bulk samples, we performed 10 min at a sintering temperature (T_S) of 1223–1233 K, at which the degree of shrinkage was saturated. Table 1 lists T_S and bulk densities (d_{bulk}) obtained from the Archimedes method for $Al_{71}Pd_{20}(Re_{1-x}Co_x)_9$ (x = 0, 0.1, 0.2, 0.3, 0.4, 0.5). Here, the data for the sample with x = 0 are quoted from a reported paper [16].

Phase characterization of the samples was evaluated by X-ray diffraction (XRD) with Cu $K\alpha$ radiation (Mini-Flex 600; Rigaku, Inc., Akishima, Japan) and a scanning thermal probe micro-imaging apparatus (STPM-1000; Advance-Riko, Inc., Yokohama, Japan). The σ and S values were measured between 300 and 873 K by the four-probe and steady-state temperature gradient methods, respectively (ZEM-3; Advance Riko, Inc., Yokohama, Japan).

The κ_{total} value was calculated from d_{bulk}, the specific heat at constant pressure (C_P), and thermal diffusivity (λ) using the relationship $\kappa_{total} = d_{bulk} \cdot C_P \cdot \lambda$. C_P was measured using differential scanning calorimetry (DSC404-F3; NETZSCH Japan, Yokohama, Japan) and λ was measured by a light flash apparatus (LFA467-HT; NETZSCH Japan, Yokohama, Japan) from 373 to 873 K. The longitudinal (v_{long}) and transverse (v_{trans}) speeds of sound were measured by the ultrasonic pulse-echo method (Echometer 1062; Nihon Matech Corp., Tokyo, Japan). For rough estimations of the elastic moduli (Poisson's ratio (ν), Young's modulus (E), shear modulus (G), and bulk modulus (B)) for these QC samples, the following relations for isotropic materials were used for the calculations [23–25]:

$$\nu = \frac{v_{long}^2 - 2v_{trans}^2}{2\left(v_{long}^2 - v_{trans}^2\right)}, \tag{4}$$

$$E = \frac{d_{bulk} v_{long}^2 \left(3v_{long}^2 - 4v_{trans}^2\right)}{v_l^2 - v_t^2}, \tag{5}$$

$$G = d_{bulk} v_{trans}^2, \tag{6}$$

$$B = d_{bulk}\left(v_{long}^2 - \frac{4}{3}v_{trans}^2\right). \tag{7}$$

Table 1. Sintering temperature (T_S), bulk densities (d_{bulk}), calculated densities (d_{calc}), and relative densities (d_{bulk}/d_{calc}) for $Al_{71}Pd_{20}(Re_{1-x}Co_x)_9$ (x = 0 [16], 0.1, 0.2, 0.3, 0.4, 0.5).

Sample	T_S (K)	d_{bulk} (g cm^{-3})	d_{calc} (g cm^{-3})	d_{bulk}/d_{calc} (%)
x = 0 [16]	1223	6.026	6.30 [22]	95.7
x = 0.1	1233	5.924	6.17	96.0
x = 0.2	1233	5.810	6.05	96.0
x = 0.3	1233	5.656	5.92	95.5
x = 0.4	1223	5.648	5.80	97.4
x = 0.5	1223	5.517	5.67	97.3

3. Results and Discussion

The relative density of the sample with x = 0 was 95.7% [16], indicating that a dense bulk sample was fabricated by the SPS process. The ideal densities of the Co-substituted samples were calculated from d_{bulk} (relative density: ~100%, 6.30 g cm^{-3}) of the sample with x = 0 [22] and the rate of change in average atomic weight (Table 1). As a result, it was found that the dense bulk samples with relative densities of >95% were fabricated for Co-substituted samples. The overall trend of d_{bulk} decreased with increasing Co concentration x, which can be understood as decreasing the average mass by substitution of the lighter element Co for Re.

We confirmed that all synthesized bulk samples were identified as an *F*-type quasi-crystalline phase [26], as shown in Figure 1A. In the Al–Pd–Re–Co system, the formation of 2/1- or 1/1-approximant crystal was not realized, unlike in Al–Pd–Re–Ru [27] and Al–Pd–Re–Fe [16] quaternary systems. We observed peak shifting to a higher degree with increasing x, indicating that the quasi-lattice constant (a_R) decreased by Co substitution for Re (Figure 1B). This trend can be qualitatively explained by substitution of the smaller atomic radii of Co (0.125 nm) for Re (0.138 nm). However, we observed that the sample with x = 0.3 had a slight increase in a_R, which may be brought about by a composition deviation, as discussed below.

The morphology of the dense bulk samples synthesized by the SPS process did not change with varying x. To assess the sample's quality, the mapping measurements of *S* at 300 K, which is sensitive to local composition, were performed (Figure 2). As a result, homogeneous microstructures were obtained, except for the sample with x = 0.3, and

there was no secondary precipitation. These results agree with the XRD measurements. The sample with x = 0.3 had a composite microstructure consisting of p- and n-type compositions with small absolute values of S. When x increased, the carrier type changed from p- to n-type, then turned to p-type again. However, its magnitude of S for an n-type material is relatively low (-10 μV K^{-1}) for the sample with x = 0.2.

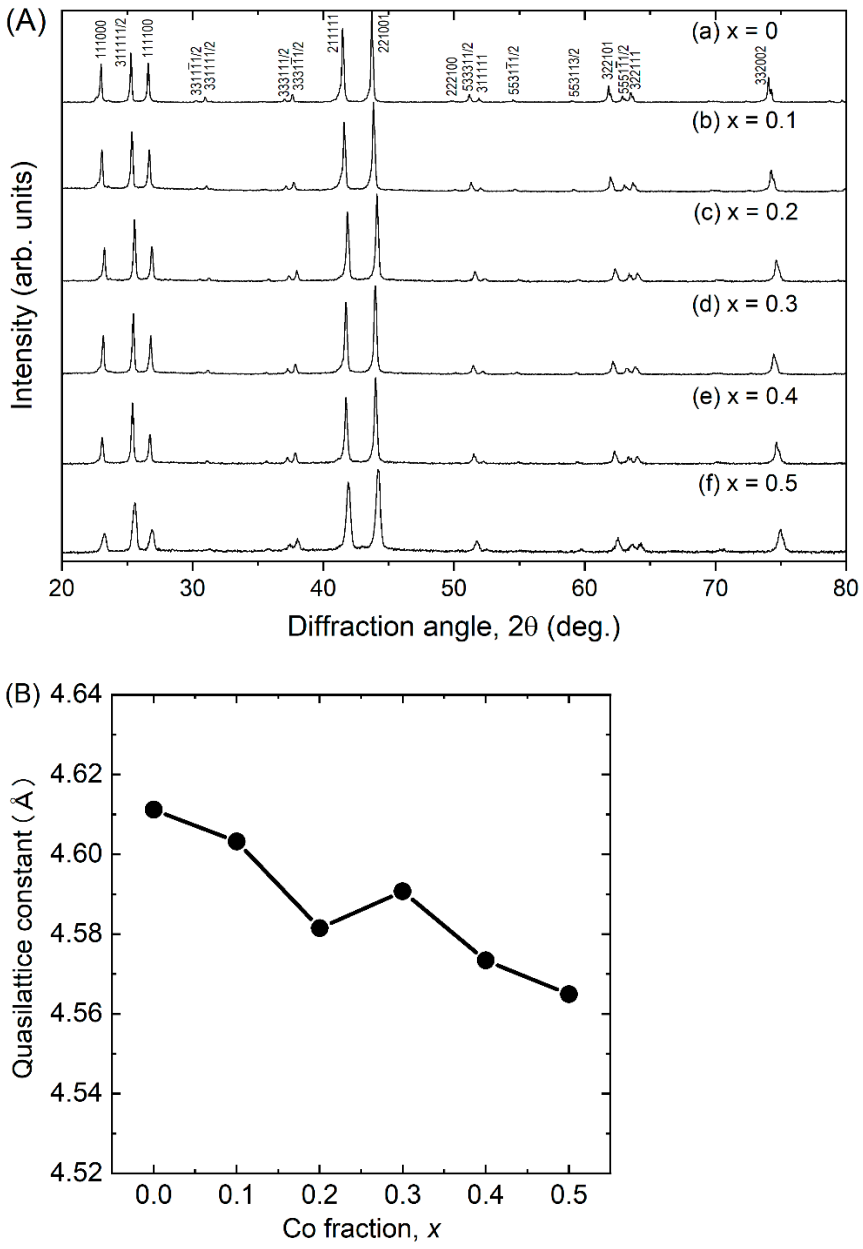


Figure 1. (**A**) X-ray diffraction patterns and (**B**) quasi-lattice constant of $Al_{71}Pd_{20}(Re_{1-x}Co_x)_9$ (x = 0 [16], 0.1, 0.2, 0.3, 0.4, 0.5).

Figure 3a–c show the temperature dependence of σ, S, and $S^2\sigma$ from 300 to 873 K for the $Al_{71}Pd_{20}(Re_{1-x}Co_x)_9$ (x = 0 [16], 0.1, 0.2, 0.3, 0.4, 0.5) samples. All samples had a similar positive temperature coefficient of σ (semiconducting behavior), with a varying magnitude of 100–280 Ω^{-1} cm^{-1} at 300 K. The calculated activation energy from the Arrhenius plot was 0.11 eV for the sample with x = 0 and increased to 0.15 eV with Co substitution. Compared with transition metal-substituted *i*-Al–Pd–Re QCs, these values are comparable with those of *i*-Al–Pd–Re–Ru QC (0.05–0.12 eV) [28] and *i*-Al–Pd–Re–Fe QC (0.14–0.17 eV) [16]. Since S at 300 K decreased owing to Co substitution for Re, the

decrease in carrier concentration was not the cause of the decrease in σ, i.e., lowering of the relaxation time owing to chemical disordering of Co at Fe sites. The absolute value of S for p-type materials (except for samples with x = 0.2 and 0.3) decreased with the increasing temperature, which is attributed to an increase in minority carriers. This is consistent with the temperature dependence of σ. The $S^2\sigma$ value showed a similar temperature dependence, with a peak at mid-temperatures of 600–700 K for all samples, and exhibited a maximum value of ~380 μW m^{-1} K^{-2} at 573 K for the unsubstituted sample, i.e., $S^2\sigma$ was not improved by Co substitution for Re because of the reduction of S and σ.

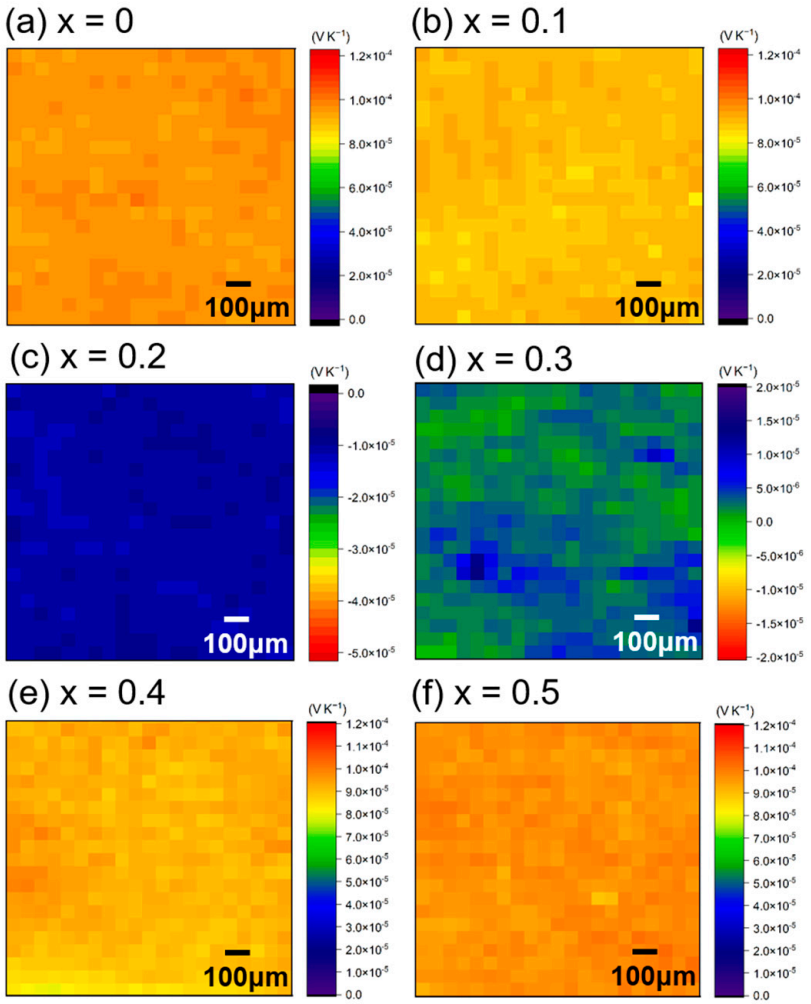


Figure 2. Seebeck coefficient mapping measurements at room temperature for $Al_{71}Pd_{20}(Re_{1-x}Co_x)_9$ (x = 0 [16], 0.1, 0.2, 0.3, 0.4, 0.5).

The highest value of σ at 300 K was measured for the *i*-$Al_{71}Pd_{20}Re_9$ QC (~280 Ω^{-1} cm^{-1}) [16]: σ decreased up to x = 0.4 and then increased for the sample with x = 0.5. This non-monotonic change in σ with varying x cannot be understood only in terms of the change in carrier concentration from the S measurement. Initially, we expected Co to be an n-type dopant and tried to replace it with Re. As expected, the S value of the sample with x = 0.2 showed n-type values (−10 μV K^{-1} at 300 K), but this changed to p-type with increasing x and its absolute value improved to 100 μV K^{-1} at 300 K for the sample with x = 0.5, which is close to that of the undoped sample (x = 0) [16]. These changes of σ and S suggest that a simple rigid-band approximation is not applicable to this system. As a result, we did not succeed in fabricating the desired n-type material with a high S.

The Co-substitution concentration dependence of σ and S is a rather complicated change and differs from those reported in previous studies on Ru [27] and Fe [28] substitu-

tion. Mizutani et al. reported an electron per atom ratio (e/a) for elements in the Periodic Table [29]: e/a = 1.31 for Re and e/a = 1.11 for Co. Using these e/a values of the constituent elements, the e/a value of *i*-Al–Pd–Re–Co QCs decreases with increasing Co concentration and, thus, E_F shifts to a lower energy, which seems to be an opposite way to obtain an n-type material. In contrast, in dilute substitution amounts of x = 0.1 and 0.2, Co appears to function as an n-type dopant. Hall coefficient measurements may clarify the underlying mechanism; however, the Hall voltage of *i*-Al–Pd–Re QC is too low to obtain reliable data at this stage.

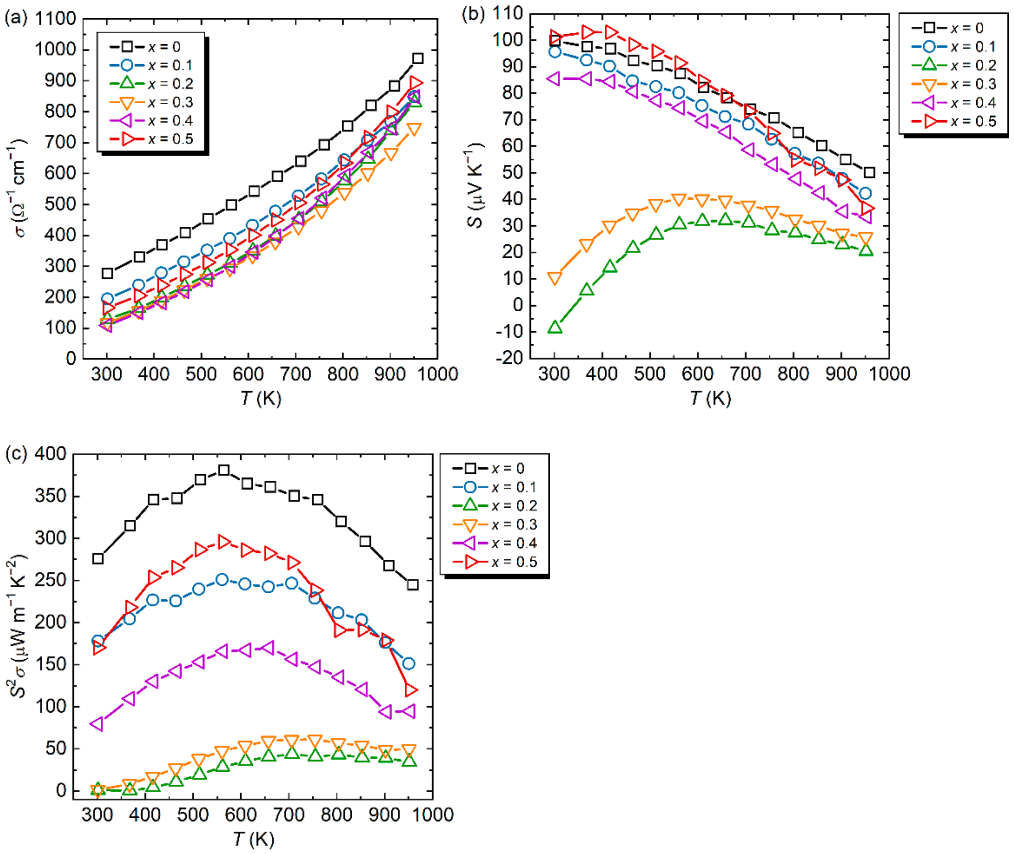


Figure 3. (**a**) Electrical conductivity (σ), (**b**) Seebeck coefficient (S), and (**c**) power factor ($S^2\sigma$) as functions of temperature for $Al_{71}Pd_{20}(Re_{1-x}Co_x)_9$ (x = 0 [16], 0.1, 0.2, 0.3, 0.4, 0.5).

The temperature dependences of C_P, λ, and κ_{total} from 373 to 973 K for all samples are shown in Figure 4a–c. The C_P values of the Al–Pd–Re–Co QCs were distributed between 0.39 and 0.41 J g^{-1} K^{-1} at 373 K and increased with the increasing temperature. The λ values at 373 K for all samples showed similar values of 0.40–0.42 mm^2 s^{-1} and a temperature dependence. Table 2 lists κ_{total} at 373 K ($\kappa_{total,373K}$) for all samples investigated. The $\kappa_{total,373K}$ value decreased from 1.28 (x = 0) to 1.08 W m^{-1} K^{-1} (x = 0.3), probably due to the large decrease in σ, as shown in Figure 3a. Regarding the estimation of $\kappa_{electron}$, the well-known Wiedemann–Franz law is not suited for QCs because it assumes that the spectral conductivity varies linearly with energy [30]. Maciá has discussed the validity of the Wiedemann–Franz law for QCs [31]. There is no empirical relationship to calculate $\kappa_{electron}$ for QCs; thus, we adopted the conventional relationship shown in Equation (8) and L_0 values using an empirical model (L_0 = 1.5 + exp[$-|S|/116$] × 10^{-8} V^2 K^{-2}) by Kim et al. [32] for a rough estimation of κ_{phonon}:

$$\kappa_{phonon} = \kappa_{total} - L_0 \sigma T. \quad (8)$$

The calculated κ_{phonon} as a function of temperature is shown in Figure 4d, and we list κ_{phonon} at 373 K ($\kappa_{phonon,373K}$) for all samples in Table 2, together with the minimum thermal conductivity at 373 K ($\kappa_{min,373K}$) using the Cahill model [33,34], which provides the lower limit of κ_{phonon} for amorphous solids and disordered crystals. The κ_{min} value can be calculated as follows:

$$\kappa_{min} = \left(\frac{\pi}{6}\right)^{\frac{1}{3}} k_B n^{\frac{2}{3}} \sum_{long,trans} v_{long,trans} \left(\frac{T}{\theta_{long,trans}}\right)^2 \int_0^{\frac{\theta_{long,trans}}{T}} \frac{x^3 e^x}{(e^x-1)^2} dx. \quad (9)$$

Here, k_B is the Boltzmann constant, n is the number density of atoms, and $\theta_{long,trans}$ is the cut-off temperature, which is given by $\theta_{long,trans} = v_{long,trans}\left(\frac{\hbar}{k_B}\right)(6\pi^2 n)^{\frac{1}{3}}$, where $\hbar$ is Planck's constant. It should be noted that the apparent increase in κ_{phonon} at high temperatures, including for the Co-substituted samples, originates from conduction carriers [30]. The $\kappa_{phonon,373K}$ was suppressed to 0.94 W m^{-1} K^{-1} by Co substitution, which is attributed to decreasing the phonon relaxation time (τ_{phonon}):

$$\kappa_{phonon} = \frac{1}{3} C_V v_s^2 \tau_{phonon}, \quad (10)$$

where C_v and v_s are the specific heat at constant volume and the effective speed of sound, respectively. Here, the C_V [35] and v_s can be expressed as:

$$C_V = C_P - 9VB\alpha^2 T; \quad (11)$$

$$v_s = \left[\frac{1}{3}\left(\frac{1}{v_{long}^3} + \frac{2}{v_{trans}^3}\right)\right]^{-1/3}, \quad (12)$$

where V and α are the atomic volume and the linear thermal expansion coefficient, respectively. Although we have no information on α for the present *i*-Al–Pd–Re–Co QCs, qualitative changes are discussed using C_P.

Table 2. Total thermal conductivity at 373 K ($\kappa_{total,373K}$), phonon thermal conductivity at 373 K ($\kappa_{phonon,300K}$), minimum thermal conductivity at 373 K ($\kappa_{min,373K}$), longitudinal (v_{long}) and transverse (v_{trans}) speeds of sound, effective speed of sound (v_s), rate of change in v_s ($\Delta v_s/v_s$), specific heat at constant pressure at 373 K ($C_{P,373K}$), and rate of change in $C_{P,373K}$ ($\Delta C_{P,373K}/C_{P,373K}$) for $Al_{71}Pd_{20}(Re_{1-x}Co_x)_9$ (x = 0 [16], 0.1, 0.2, 0.3, 0.4, 0.5).

Sample	$\kappa_{total,373K}$	$\kappa_{phonon,373K}$	$\kappa_{min,373K}$	v_{long}/v_{trans}
	(W m^{-1} K^{-1})	(W m^{-1} K^{-1})	(W m^{-1} K^{-1})	(m s^{-1})
x = 0 [16]	1.28	1.05	1.05	6430/3420
x = 0.1	1.27	1.09	1.07	6400/3500
x = 0.2	1.16	1.01	1.09	6430/3660
x = 0.3	1.08	0.94	1.06	6370/3490
x = 0.4	1.25	1.14	1.09	6480/3590
x = 0.5	1.15	1.00	1.11	6690/3660
Sample	v_s	$\Delta v_s/v_s$	$C_{P,373K}$	$\Delta C_{P,373K}/C_{P,373K}$
	(m s^{-1})	(%)	(J g^{-1} K^{-1})	(%)
x = 0 [16]	3820	-	0.3997	-
x = 0.1	3900	2.1	0.4138	3.5
x = 0.2	4070	6.5	0.4249	6.3
x = 0.3	3890	1.8	0.3902	−2.4
x = 0.4	4000	4.7	0.4124	3.1
x = 0.5	4080	6.8	0.3903	2.4

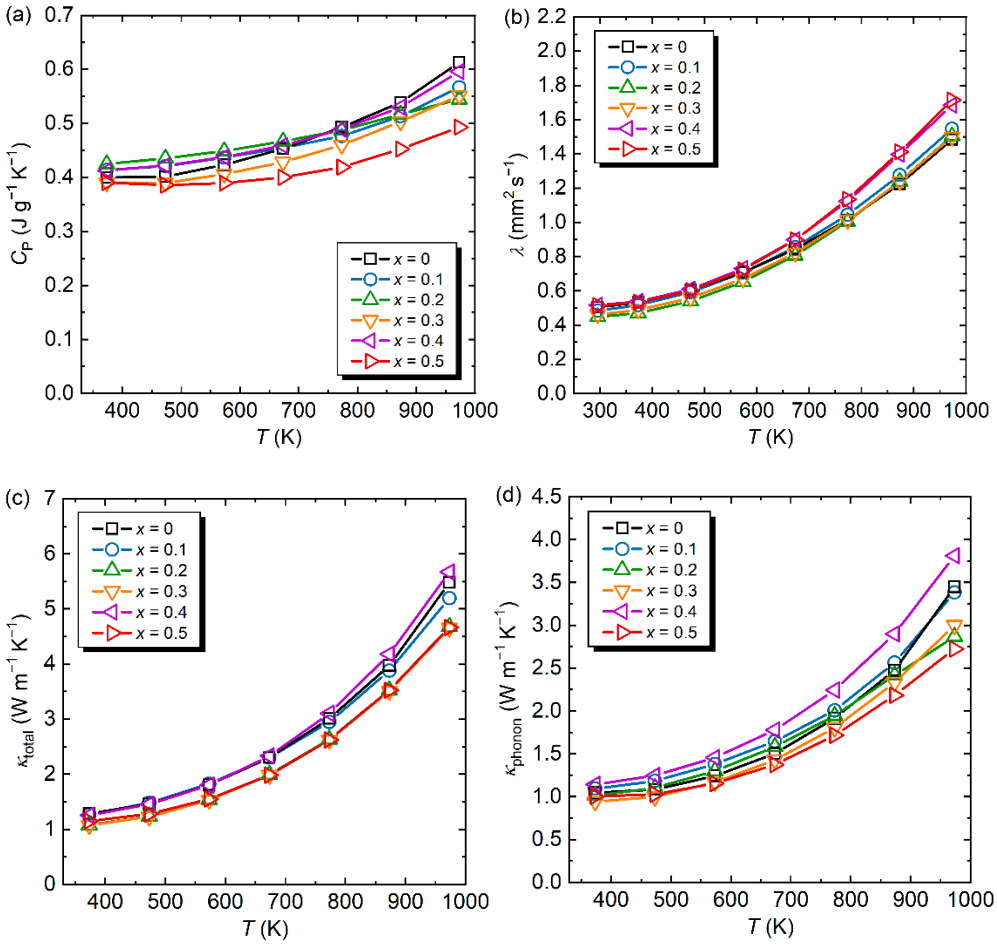


Figure 4. (**a**) Specific heat at constant pressure (C_P), (**b**) thermal diffusivity (λ), (**c**) total thermal conductivity (κ_{total}), and (**d**) phonon thermal conductivity (κ_{phonon}) as functions of temperature for $Al_{71}Pd_{20}(Re_{1-x}Co_x)_9$ (x = 0 [16], 0.1, 0.2, 0.3, 0.4, 0.5).

Co-substitution for Re could reduce $\kappa_{phonon,373K}$ from 1.05 (x = 0) to 0.94 (x = 0.3) W m^{-1} K^{-1}, i.e., up to a 10% reduction. The C_P and v_s values did not change significantly between samples with x = 0 and 0.3 (less than ~2% for each) (Table 2), so τ_{phonon} is likely reduced because of the alloying effect. Here, we note that $\kappa_{phonon,373K}$ of the sample with x = 0 is the same as the $\kappa_{min,373K}$ value, and the observed $\kappa_{min,373K} > \kappa_{phonon,373K}$ relationship is attributed to overestimation of L_0 [36]. This trend was also observed in the Al–Pd–Re–Fe quaternary system [16].

The estimated elastic parameters of ν, E, G, and B for $Al_{71}Pd_{20}(Re_{1-x}Co_x)_9$ (x = 0, 0.1, 0.2, 0.3, 0.4, 0.5) are listed in Table 3. The general mechanical properties of QCs are hard and brittle, so the estimated elastic moduli are consistent with the general trend. There is no literature on the mechanical properties of *i*-Al–Pd–Re QC. In general, an arc-melted and annealed *i*-Al–Pd–Re sample has a porous microstructure of a relative density of <70% because *i*-Al–Pd–Re QC forms from the peritectic reaction of Al_3Pd_2 and $Al_{11}Re_4$, and thus is very fragile [22]. We speculate that such a porous sample makes it difficult to measure intrinsic mechanical properties. The sintered bulk samples of *i*-Al–Pd–Re(–Co) QCs were dense enough to measure their intrinsic mechanical properties. Indeed, we obtained a higher B value of over 150 GPa for the sample with x = 0, which is close to Fe-based thermoelectric materials of $Fe_3Al_2Si_3$, β-$FeSi_2$, and $FeAl_2$ [37]. It was found that Co substitution for Re slightly reduced the elastic moduli of ν, E, G, and B. The ν value is related to the volume change in the uniaxial deformation. Classical elastic theory predicts ν to be −1 to 0.5. A larger ν value means that a material possesses better plasticity. The estimated ν values of 0.260–0.303 for *i*-Al–Pd–Re–Co QCs are between those of ionic

materials, such as NaCl (ν = 0.253) and CsCl (ν = 0.266) [38], and metallic materials, such as Aluminum 6061-T6 (ν = 0.33) and Cu (ν = 0.355) [38]. This may indicate that Co substitution for Re gives *i*-Al–Pd–Re QC a more ionic and brittle character. Compared with other *i*-QCs, such as *i*-Al–Pd–Mn QC [39,40] and *i*-Al–Cu–Fe QC [39], *i*-Al–Pd–Re–Co QCs had higher ν and B values, but the G value was almost identical. Decreasing ν will be associated with increasing covalency between atoms because covalent materials such as diamond and cubic boron nitride have low ν values of 0.069 and 0.14–0.18, respectively [38].

Table 3. Estimated elastic moduli (Poisson's ratio (ν), Young's modulus (E), shear modulus (G), and bulk modulus (B)) for $Al_{71}Pd_{20}(Re_{1-x}Co_x)_9$ (x = 0, 0.1, 0.2, 0.3, 0.4, 0.5), and those of *i*-Al–Pd–Mn [39,40] and *i*-Al–Cu–Fe [39] QCs.

Sample	ν	E	G	B
	(-)	(GPa)	(GPa)	(GPa)
x = 0	0.303	184	70.5	155
x = 0.1	0.287	187	72.6	146
x = 0.2	0.260	196	77.8	136
x = 0.3	0.286	177	68.9	138
x = 0.4	0.279	186	72.8	140
x = 0.5	0.286	190	73.9	148
i-Al–Pd–Mn [39]	0.254	-	72.4	123
i-Al–Pd–Mn [40]	0.256	-	70.4	121
i-Al–Cu–Fe [39]	0.232	-	68.1	104

Finally, we briefly mention zT as a function of temperature, as shown in Figure 5. The maximum zT value (zT_{max}) was 0.12 at 573 K for the sample with x = 0. Although κ_{total} was reduced by the alloying effect via Co substitution for Re, zT_{max} was not enhanced because of the lowering of $S^2\sigma$ for all measured temperature ranges.

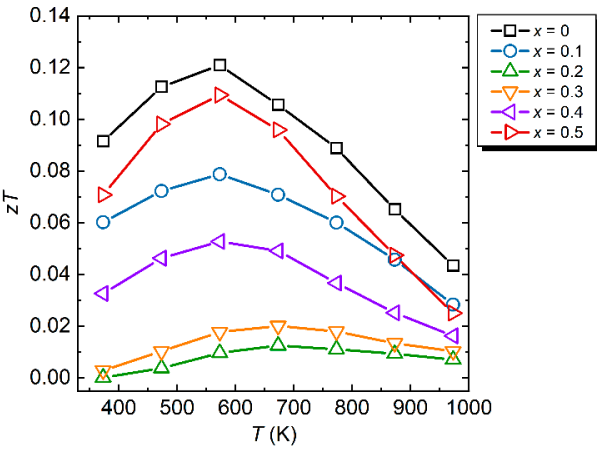


Figure 5. Dimensionless figure of merit (zT) as a function of temperature for $Al_{71}Pd_{20}(Re_{1-x}Co_x)_9$ (x = 0 [16], 0.1, 0.2, 0.3, 0.4, 0.5).

4. Conclusions

In this study, we systematically investigated the effect of Co substitution for Re for *i*-Al–Pd–Re QC on thermoelectric and mechanical properties. We found that the icosahedral quasi-crystalline phase can be synthesized by 50% replacement of Co for Re. Although κ_{total} was reduced by the alloying effect via Co substitution for Re, zT_{max} was not enhanced because of the lowering of $S^2\sigma$ for all measured temperature ranges. Co could produce n-type carriers in dilute substitution amounts of x = 0.1 and 0.2; however, S at 300 K showed an n- to p-type transition with increasing x. The observed effects of Co concentration on σ and S showed a complicated change, suggesting that a simple rigid-band approximation is not applicable to *i*-Al–Pd–Re QC. To develop a robust thermoelectric power generation

module using Al-based QCs, we need to synthesize a high-performance n-type QC. This is a future challenge for the practical application of QCs.

Funding: This work was supported by KAKENHI (Grant No. 19H05821, 20H02469) from the Japan Society for the Promotion of Science (JSPS).

Institutional Review Board Statement: Not applicable.

Informed Consent Statement: Not applicable.

Data Availability Statement: The data presented in this study are available upon reasonable request from the corresponding author.

Acknowledgments: The author (Y.T.) acknowledges Noriko Iijima for support on synthesis and characterization. We thank Kathryn Sole for editing a draft of this manuscript.

Conflicts of Interest: The authors declare no conflict of interest.

References

1. Freer, R.; Ekren, D.; Ghosh, T.; Biswas, K.; Qiu, P.; Wan, S.; Chen, L.; Han, S.; Fu, C.; Zhu, T.; et al. Key properties of inorganic thermoelectric materials-tables (version 1). *J. Phys. Energy* **2022**, *4*, 022002. [CrossRef]
2. Shi, X.-L.; Zou, J.; Chen, Z.-G. Advanced Thermoelectric Design: From Materials and Structures to Devices. *Chem. Rev.* **2020**, *120*, 7399–7515. [CrossRef]
3. Zevalkink, A.; Smiadak, D.M.; Blackburn, J.L.; Ferguson, A.J.; Chabinyc, M.L.; Delaire, O.; Wang, J.; Kovnir, K.; Marin, J.; Schelhas, L.T.; et al. A practical field guide to thermoelectrics: Fundamentals, synthesis, and characterization. *Appl. Phys. Rev.* **2018**, *5*, 021303. [CrossRef]
4. Beretta, D.; Neophytou, N.; Hodges, J.M.; Kanatzidis, M.G.; Narducci, D.; Martin-Gonzalez, M.; Beekman, M.; Balke, B.; Cerretti, G.; Tremel, W.; et al. Thermoelectrics: From history, a window to the future. *Mater. Sci. Eng. Rep.* **2019**, *138*, 210–255. [CrossRef]
5. Xin, J.; Tang, Y.; Liu, Y.; Zhao, X.; Pan, H.; Zhu, T. Valleytronics in thermoelectric materials. *NPJ Quantum Mater.* **2018**, *3*, 9. [CrossRef]
6. Kanatzidis, M.G. Nanostructured thermoelectrics: The new paradigm? *Chem. Mater.* **2010**, *22*, 648–659. [CrossRef]
7. Prauzek, M.; Konecny, J.; Borova, M.; Janosova, K.; Hlavica, J.; Musilek, P. Energy Harvesting Sources, Storage Devices and System Topologies for Environmental Wireless Sensor Networks: A Review. *Sensors* **2018**, *18*, 2446. [CrossRef]
8. Takagiwa, Y.; Ikeda, T.; Kojima, H. Earth-Abundant Fe-Al-Si Thermoelectric (FAST) Materials: From Fundamental Materials Research to Module Development. *ACS Appl. Mater. Interfaces* **2020**, *12*, 48804–48810. [CrossRef] [PubMed]
9. Takagiwa, Y.; Hou, Z.; Tsuda, K.; Ikeda, T.; Kojima, H. Fe–Al–Si Thermoelectric (FAST) Materials and Modules: Diffusion-Couple and Machine-Learning Assisted Materials Development. *ACS Appl. Mater. Interfaces* **2021**, *13*, 53346–53354. [CrossRef]
10. Dolinšek, J. Electrical and thermal transport properties of icosahedral and decagonal quasicrystals. *Chem. Soc. Rev.* **2012**, *41*, 6730–6744. [CrossRef]
11. Dubois, J.-M. Properties and applications of quasicrystals and complex metallic alloys. *Chem. Soc. Rev.* **2012**, *41*, 6760–6777. [CrossRef] [PubMed]
12. Singh, A. Tailoring microstructure of Mg–Zn–Y alloys with quasicrystal and related phases for high mechanical strength. *Sci. Technol. Adv. Mater.* **2014**, *15*, 044803. [CrossRef] [PubMed]
13. Takeuchi, T. Very large thermal rectification in bulk composites consisting partly of icosahedral quasicrystals. *Sci. Technol. Adv. Mater.* **2014**, *15*, 064801. [CrossRef] [PubMed]
14. Takagiwa, Y.; Kimura, K. Metallic-covalent bonding conversion and thermoelectric properties of Al-based icosahedral quasicrystals and approximants. *Sci. Technol. Adv. Mater.* **2014**, *15*, 044802. [CrossRef] [PubMed]
15. Maćia, E. Thermoelectric figure of merit of AlPdRe icosahedral quasicrystals: Composition-dependent effects. *Phys. Rev. B* **2004**, *69*, 184202. [CrossRef]
16. Takagiwa, Y.; Kimura, K. Reinvestigation of the Thermoelectric Properties of Fe-Substituted Icosahedral Al–Pd–Re Quasicrytals. *Phys. Status Solidi A* **2022**, *219*, 2200073. [CrossRef]
17. Trambly de Laissardière, G.; Nguyen-Manh, N.; Mayou, D. Electronic structure of complex Hume-Rothery phases and quasicrystals in transition metal aluminides. *Prog. Mater. Sci.* **2005**, *50*, 679–788. [CrossRef]
18. Steurer, W. Why are quasicrystals quasiperiodic? *Chem. Soc. Rev.* **2012**, *41*, 6719–6729. [CrossRef]
19. Takagiwa, Y.; Kamimura, T.; Okada, J.T.; Kimura, K. Thermoelectric Properties of Icosahedral Al–Pd–(Mn or Re) Quasicrystals: Improvement of the *ZT* Value by Ga Substitution for Al Atoms. *J. Electron. Mater.* **2010**, *39*, 1885–1889. [CrossRef]
20. Takagiwa, Y.; Kamimura, T.; Hosoi, S.; Okada, J.T.; Kimura, K. Thermoelectric properties of polygrained icosahedral $Al_{71-x}Ga_xPd_{20}Mn_9$ (x = 0, 2, 3, 4) quasicrystals. *J. Appl. Phys.* **2008**, *104*, 073721. [CrossRef]
21. Iwasaki, Y.; Kashimura, T.; Kitahara, K.; Kimura, K. Possibility of Semiconducting Electronic Structure on AlPdCo 1/1 Cubic Quasicrystalline Approximant. *Mater. Trans.* **2021**, *62*, 317–320. [CrossRef]

22. Takagiwa, Y.; Kamimura, T.; Hosoi, S.; Okada, J.T.; Kimura, K. Thermoelectric properties of Al–Pd–Re quasicrystal sintered by Spark Plasma Sintering (SPS): Effect of improvement of microstructure. *Z. Kristallogr.* **2009**, *224*, 79–83. [CrossRef]
23. Birch, F. Finite Elastic Strain of Cubic Crystals. *Phys. Rev.* **1947**, *71*, 809–824. [CrossRef]
24. Anderson, O.L. A simplified method for calculating the debye temperature from elastic constants. *J. Phys. Chem. Solids* **1963**, *24*, 909–917. [CrossRef]
25. Shiota, Y.; Muta, H.; Yamamoto, K.; Ohishi, Y.; Kurosaki, K.; Yamanaka, S. A new semiconductor $Al_2Fe_3Si_3$ with complex crystal structure. *Intermetallics* **2017**, *89*, 51–56. [CrossRef]
26. Stadnik, Z.M.; Zhang, G.W.; Tsai, A.-P.; Inoue, A. Electronic structure of icosahedral $Al_{65}Cu_{20}Ru_{15}$ studied by photoemission spectroscopy. *Phys. Rev. B* **1995**, *81*, 4023–4041. [CrossRef] [PubMed]
27. Nagata, T.; Kirihara, K.; Kimura, K. Effect of Ru substitution for Re on the thermoelectric properties of AlPdRe icosahedral quasicrystals. *J. Appl. Phys.* **2003**, *94*, 6560–6565. [CrossRef]
28. Okada, J.T.; Hamamatsu, T.; Hosoi, S.; Nagata, T.; Kimura, K. Improvement of thermoelectric properties of icosahedral AlPdRe quasicrystals by Fe substitution for Re. *J. Appl. Phys.* **2007**, *101*, 103702. [CrossRef]
29. Mizutani, U.; Sato, H.; Inukai, M.; Zijlstra, E.S. e/a determination for 4d- and 5d-transition metal elements and their intermetallic compounds with Mg, Al, Zn, Cd and In. *Philos. Mag.* **2013**, *93*, 3353–3390. [CrossRef]
30. Takeuchi, T. Unusual Increase of Electron Thermal Conductivity Caused by a Pseudogap at the Fermi Level. *J. Electron. Mater.* **2009**, *38*, 1354–1359. [CrossRef]
31. Maciá, E.; Rodríguez-Oliveros, R. Theoretical assessment on the validity of the Wiedemann-Franz law for icosahedral quasicrystals. *Phys. Rev. B* **2007**, *75*, 104210. [CrossRef]
32. Kim, H.-S.; Gibbs, Z.M.; Tang, Y.; Wang, H.; Snyder, G.J. Characterization of Lorenz number with Seebeck coefficient measurement. *APL Mater.* **2015**, *3*, 041506. [CrossRef]
33. Cahill, D.G.; Pohl, R.O. Heat flow and lattice vibrations in glasses. *Solid State Commun.* **1989**, *70*, 927–930. [CrossRef]
34. Cahill, D.G.; Watson, S.K.; Pohl, R.O. Lower limit to the thermal conductivity of disordered crystals. *Phys. Rev. B* **1992**, *46*, 6131–6140. [CrossRef]
35. Fukushima, K.; Suyama, H.; Tokumoto, Y.; Kamimura, Y.; Takagiwa, Y.; Edagawa, K. Comparative study of high-temperature specific heat for Al-Pd-Mn icosahedral quasicrystals and crystal approximants. *J. Phys. Commun.* **2021**, *5*, 085002. [CrossRef]
36. Putatunda, A.; Singh, D.J. Lorenz number in relation to estimates based on the Seebeck coefficient. *Mater. Today Phys.* **2019**, *8*, 49–55. [CrossRef]
37. Hou, Z.; Takagiwa, Y.; Shinohara, Y.; Xu, Y.; Tsuda, K. First-principles study of electronic structures and elasticity of $Al_2Fe_3Si_3$. *J. Phys. Condens. Matter* **2021**, *33*, 195501. [CrossRef]
38. Mott, P.H.; Roland, C.M. Limits to Poisson's ratio in isotropic materials. *Phys. Rev. B* **2009**, *80*, 132104. [CrossRef]
39. Tanaka, K.; Mitarai, Y.; Koiwa, M. Elastic constants of Al-based icosahedral quasicrystals. *Philos. Mag.* **1996**, *73*, 1715–1723. [CrossRef]
40. Duquesne, J.-Y.; Perrin, B. Elastic wave interaction in icosahedral AlPdMn. *Phys. B* **2002**, *316*, 317–320. [CrossRef]